Versão do arquivo anexado / Version of attached file:

Versão do Editor / Published Version

Mais informações no site da editora / Further information on publisher's website:

https://aip.scitation.org/doi/10.1063/1.4766450

DOI: 10.1063/1.4766450

Direitos autorais / Publisher's copyright statement:

Ferroic states and phase coexistence in BiFeO₃-BaTiO₃ solid solutions

R. A. M. Gotardo,[1] D. S. F. Viana,[1] M. Olzon-Dionysio,[1] S. D. Souza,[1] D. Garcia,[1] J. A. Eiras,[1] M. F. S. Alves,[2] L. F. Cótica,[2] I. A. Santos,[2] and A. A. Coelho[3]
[1]*Departamento de Física, Universidade Federal de São Carlos, Rod. Washington Luiz, Km 235, São Carlos–São Paulo 13565-345, Brazil*
[2]*Departamento de Física, Universidade Estadual de Maringá, Av. Colombo, 5790, Maringá–Paraná 87020-900, Brazil*
[3]*Departamento de Física Aplicada, Universidade Estadual de Campinas, Instituto de Física Gleb Wataghin, Barão Geraldo, Campinas–São Paulo 13083-970, Brazil*

In this paper structural, electric, magnetic, and Mössbauer spectroscopy studies were conducted in (x)BiFeO₃–(1-x)BaTiO₃, $0.9 \geq x \geq 0.3$, solid solutions. X-ray diffraction and Rietveld refinement studies indicated the formation of single-phased materials crystallized in a distorted perovskite structure with the coexistence of rhombohedral and monoclinic symmetries. Room temperature ferroelectric hysteresis loops showed that the electric polarization increases with the increase of the BaTiO₃ content due to the singular structural evolution of the studied solid solutions. All samples presented weak ferromagnetic ordering, which indicates that the BaTiO₃ substitution in the BiFeO₃ matrix released the latent magnetization. Mössbauer studies revealed a magnetic spectral signature corresponding to ordered Fe^{3+} ions, and a decrease of the magnetic hyperfine magnetic fields with the increase of the BaTiO₃ content. The composition 0.3BiFeO₃–0.7BaTiO₃ presented a spectral signature corresponding to a paramagnetic behavior, which strongly suggests that the observed magnetization in this sample is due to the Ti^{3+} ions. © *2012 American Institute of Physics.*
[http://dx.doi.org/10.1063/1.4766450]

I. INTRODUCTION

The magnetic and electric properties of advanced materials are essential in modern technologies and the search for compounds where these two ferroic properties coexist in a way that a unique device can perform more than one task is of great technological importance. Such multifunctional materials, that combine these two or more ferroic properties in the same phase, are called multiferroics.[1,2] Indeed, some of these materials can present a coupling between the magnetic and electric properties. Examples of this coupling are the magnetoelectric effect, the induction of a magnetization by an electric field or a polarization by a magnetic field, and the control of the polarization direction by a magnetic field, or vice versa, through the Dyzialonshinski-Morya interaction.[3,4] Such coupling provides a new degree of freedom for devices design and can be used to construct new multifunctional devices, such as: electric field-controlled magnetic data storage, magnetic sensors, transducers, quantum electro-magnets, and spintronic ones.[5,6]

Majority of multiferroic magnetoelectric materials present a very low coupling between their order parameters.[5,6] In fact, the bismuth ferrite (BiFeO₃–BF) is one which presents a microscopic coupling between the magnetic and electric ordering at room temperature.[7] The BF ferroelectric and antiferromagnetic phase transition temperatures are significantly above room temperature ($T_C \sim 750\,°C$ (Ref. 8) and $T_N \sim 370\,°C$ (Refs. 9 and 10)). Bulk BF crystallizes in a rhombohedral distorted perovskite structure described by *R3c* space group, with the ferroelectricity arising mainly from the Bi 6s lone pairs.[11,12] The partially filled d orbital of Fe ions

lead to a G–type antiferromagnetic spin configuration with a canted structure due to the Dzyaloshinskii–Moriya interaction,[5,13] which should induce a weak-ferromagnetic ordering. Moreover, BF also presents an incommensurate cycloidal spin structure with a long-range period (∼62 nm) which cancels the net macroscopic magnetization.[5,13,14] However, some drawbacks of BF are the low resistivity and the difficult to synthetize single-phased polycrystalline samples. This way, one approach for overcoming these problems is the synthesis of solid solutions with other perovskite materials, especially with BaTiO₃ (BT) and PbTiO₃ (PT).[15–17]

BT substituted BF compounds, forming (x)BiFeO₃–(1-x)BaTiO₃ (BF–BT) solid solutions, are reported to release the macroscopic magnetization of the BF matrix,[18,19] enhancing the electrical resistivity,[18] ferroelectricity,[20] weak-ferromagnetic ordering interactions,[15,19] and also the piezoelectricity.[21] The BF–BT crystal structures were reported by Kumar *et al.*[18] as changing from rhombohedral to cubic symmetries for $0.1 < x < 0.7$, and then to a tetragonal symmetry for $x < 0.1$. However, Kim *et al.*[19] reported, from neutron diffraction studies, a non-centrosymmetric tetragonal symmetry for $x < 0.6$. In fact, the substitution of Ba^{+2} for Bi^{+3} and Ti^{4+} for Fe^{3+} lead to more complex structural changes. Once, that the ionic radii of Ba^{+2} is larger than the one of Bi^{+3}, 1.56 and 1.17 Å, respectively. These differences induce isostatic pressure (chemical pressure) on the crystal cells. Actually, it is reported a change of the BF crystal symmetry by applying isostatic pressure, where the symmetry evolves to monoclinic[22] or orthorrhombic[23,24] arrangements. Recently, it was also reported a monoclinic symmetry (*Cc* space group) for the BF–PT system at the

morphotropic phase boundary,[25] as well as the coexistence of rhombohedral and tetragonal,[26] or cubic[20] and monoclinic[15] symmetries for BF–BT solid solutions.

It is also worth noting that in BF–BT solid solutions two competing mechanisms for ferroelectricity coexist, i.e., the lone pair of the Bi atoms that shifts the Fe/Ti ion in the [111] direction[1,12] and the Ti–O covalent bond in the [001] direction. In fact, these are the individual mechanisms for ferroelectricity existence in BF and BT compounds, respectively. Similar competing mechanisms are reported for $Pb(Zr_{1-x}Ti_x)O_3$ (PZT) ceramics with x = 0.48,[27] where the coexistence of tetragonal and monoclinic symmetries is currently reported.[27,28] In this compounds, the polarization of the monoclinic symmetry lies along a direction between [001] and [111] pseudo-cubic directions, where the monoclinic symmetry represents a bridge between the rhombohedral and tetragonal systems.[27,28] In this context, investigations focusing the understanding of the close relation between structure and ferroic sates in BF–BT solid solutions seems to be imperative mainly due to their fascinating physics and the peculiar potentialities for practical applications.

Thus, in this paper structural, ferroelectric, and magnetic studies were conducted in BF–BT solid solutions processed by high-energy ball milling. Our results point to the formation of perovskite structured materials where the competing mechanisms for ferroelectricity in [111] and [001] directions lead to the coexistence of rhombohedral (*R3c*) and monoclinic (*Cm*) phases for all studied compositions. It was found that the observed ferroic properties are directly related to the observed structural changes promoted in the BF matrix by addition of the BT compound.

II. EXPERIMENTAL

Polycrystalline $(x)BiFeO_3–(1-x)BaTiO_3$ (BF–BT) samples were processed by high-energy ball milling in a Retsch PM 100 planetary ball mill by using analytical grade (Aldrich) bismuth oxide (Bi_2O_3), iron oxide (Fe_2O_3), and barium titanate (BT) as starting materials as previously reported.[15,29] Following the batching formula, the powders were ball milled for 3 h and annealed at 1023 K for 1 h. The synthesized samples were isostatically cold pressed (50 MPa) into discs, and sintered between 1253 and 1473 K for 2 h in air. X-ray diffraction (XRD) analyses of powdered ceramics were performed using a Shimadzu XRD 7000 diffractometer (Cu K_α radiation) operating in step-like mode in the 2θ range of 20°-100° in steps of 0.01°. The XRD results were refined through Rietveld analysis using the FULLPROF program.[30] Ferroelectric hysteresis loops were obtained by using a modified Sawyer–Tower circuit and the magnetic hysteresis loops were performed at room temperature in a Quantum Design physical property measurement system. The Mössbauer spectroscopic characterizations were performed in the transmission geometry, using a conventional Mössbauer spectrometer in a constant acceleration mode. The γ rays were provided by a nominal 25 mCi $^{57}Co(Rh)$ source and the Mössbauer spectra were analyzed with a non-linear least-square routine, with Lorentzian line shapes. The isomer shift (IS) data are given relative to α-Fe.

III. RESULTS AND DISCUSSION

Figures 1–3 show the XRD and Rietveld refinement results for the BF–BT solid solutions studied in this work. All compositions are single-phased and crystallized in a distorted perovskite structure. Figure 1 shows the XRD data and Rietveld analyses for solid solutions with 0.8BF–0.2BT and 0.5BF–0.5BT compositions, respectively. The XRD peaks were indexed considering the coexistence of *R3c* (rhombohedral) and *Cm* (monoclinic) symmetries, by applying a recently proposed *R3c–Cm* structural model,[15,31] considering the possibilities proposed by Ravindran *et al.*[22] by DFT calculations. Also, attempts in some space groups relevant to the $BiFeO_3$–$BaTiO_3$ system (*R3c*, *R3m* and *P4mm*) and a mixture of the *R3c* with *P4mm* or *P3mn* space groups. Likewise, other monoclinic ones (*Cc* for example) indicate that the best refinement model was the *R3c-Cm*. The refined parameters and graphical analyzes indicate a complete agreement between the experimental data and the structural model. For high BF concentrations, the XRD patterns exhibit a splitting of the maximum intensity 2θ peak (hkl)-*R3c* (Figure 2), close to 31.7°, which is characteristic of a rhombohedral perovskite phase (*R3c*). As the BT concentration increases, the intensity of the peak (h1k1l1) on the right reduces and the linewidth of the peak (h2k2l2) on the left is
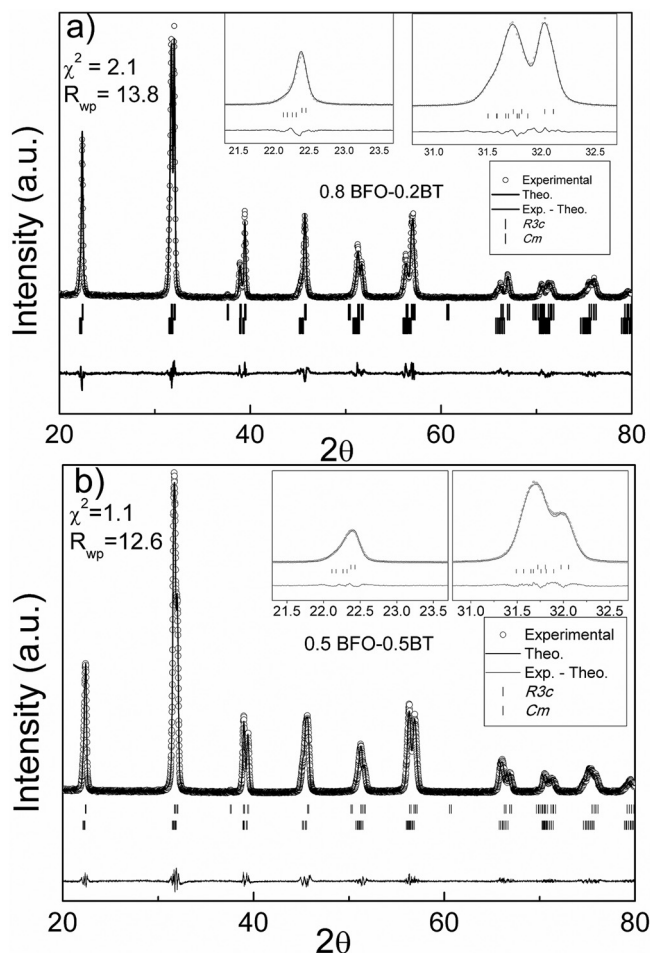

FIG. 1. X-ray diffraction patterns and Rietveld refinement results for (a) $0.8BiFeO_3–0.2BaTiO_3$ and (b) $0.5BiFeO_3–0.5BaTiO_3$ solid solutions. Inset: enlargements of the 22.5° and 32° 2θ regions.
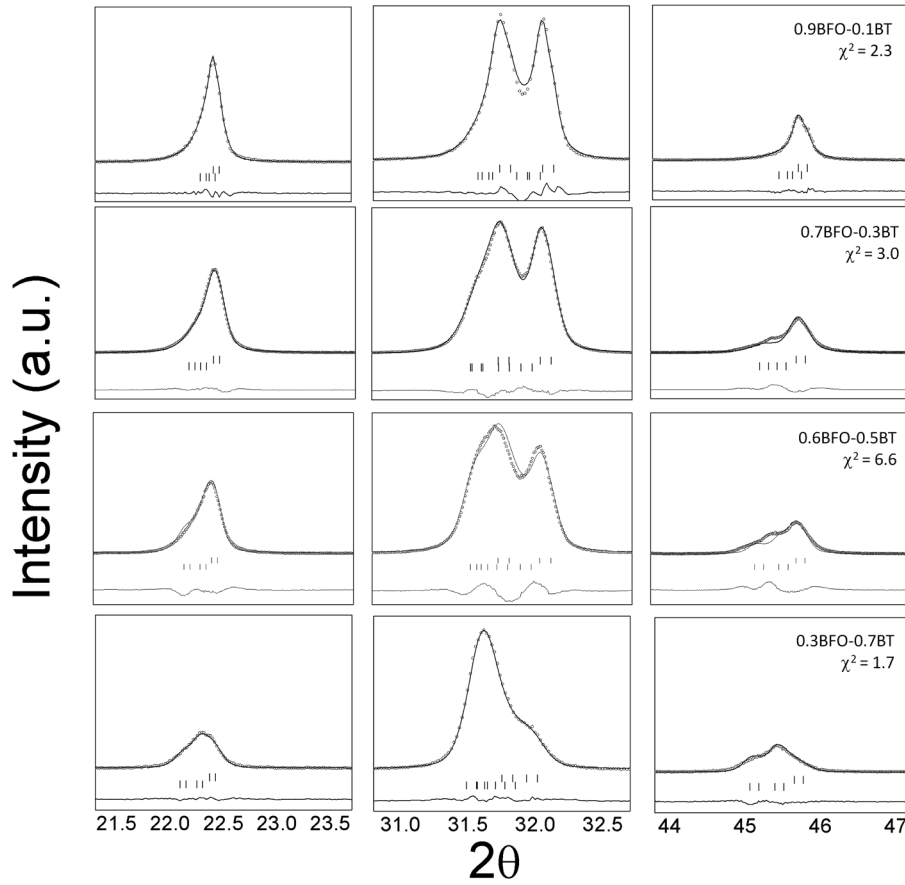
FIG. 2. X-ray diffraction patterns and Rietveld refinement results for three different 2θ regions.

broadened. These changes in the (h1k1l1) and (h2k2l2) peaks intensity and broadening is due to the increase of the *Cm* phase content by decreasing the BF content, as shown in Fig. 3(b). In fact, this broadening is also observed for 2θ (h3k3l3) and (h4k4l4) peaks near 22.25° and 45.5°, respectively (Fig. 2).

The lattice parameters also change with the increase of the BT content, as shown in Fig. 3(a), where the *a* lattice parameter for the *R3c* unit cell increases, while the *c* lattice parameter decreases with the increase of the BT concentration. Interestingly, the monoclinic β angle is nearing 90° with increasing BT content, and the *a* and *b* lattice parameters of
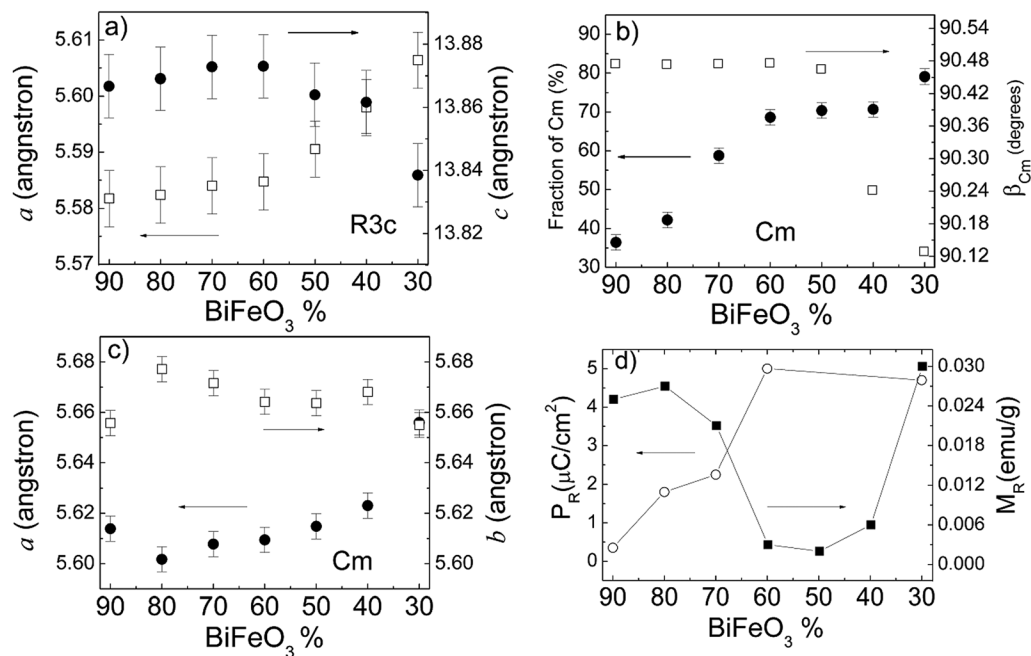

FIG. 3. (a) Lattice parameters for the *R3c* unit cell, (b) fraction of the *Cm* phase and the β monoclinic angle, (c) lattice parameters for the *Cm* unit cell, and (d) remnant polarizations and magnetizations as a function of the BiFeO$_3$ concentration.

the monoclinic unit cell are nearing one each other, becoming almost the same for x = 0.3. Interestingly, similar results are observed in PMN-PT[27] and PZT[28] systems where the symmetry also changes with temperature, from a monoclinic to a tetragonal one. As a result, the Fe/Ti–O bonds start to be the predominant distortion mechanism, and the system approaches to a tetragonal symmetry for higher BT concentrations.

The compositional evolution of the *Cm* symmetry (Fig. 3(b)) is also reflected in the ferroelectric hysteresis loops of the BF-BT solid solutions (Fig. 3(d)). P *versus* E loops for x = 0.9, 0.8, 0.7, 0.6, and 0.3, at 10 Hz and 300 K, are shown in Fig. 4. As BF is reported to present a very high polarization (60–90 μC/cm^2),[24] similar polarization levels are expected for highly BF concentrated BF–BT samples. However, solid solutions with x = 0.9 and 0.8 are reported to present only small polarizations. As ferroelectric characterizations in BF-based solid solutions are very difficult to be performed due to the low resistivity of the BF matrix ($\sim 10^6$ Ω/cm (Ref. 24)), the observed low polarizations for x = 0.9 or 0.8 samples ($\sim$1–4 μC/cm^2)[32,33] is generally assigned to conductivity effects or to the restriction in applying high electric fields during characterization. The P *versus* E results (Fig. 4) not showed any traces of spurious conductivity effects. In fact, we were able to apply high electric fields (50 and 30 kV/cm, respectively) in the samples with composition 0.9BF-0.1BT and 0.8BF-0.2BT. However, saturation was not achieved and the obtained polarization still low (1.0 and 4.0 μC/cm^2, respectively).

With further addition of BT, an increase of the polarization is observed. Similar results are also found in literature, where it was reported polarizations up to 30,[34] 42, 21, and 5 μC/cm^2 (Ref. 20) for compositions 0.7BF–0.3BT, 0.67BF–0.23BT, 0.6BF–0.4BT, and 0.5BF–0.5BT, respectively. Comparing these results with those found in literature it is observed that the polarizations of BF–BT solid solutions increase with the increase of the BT content, until reach a maximum for compositions around 0.67BF–0.23BT,[20,21] where the polarization starts to decrease. It seems clear that this behavior is intimately linked with the structural evolution of the BF–BT samples. As discussed above, in this system, the coexistence of two mechanisms for ferroelectricity
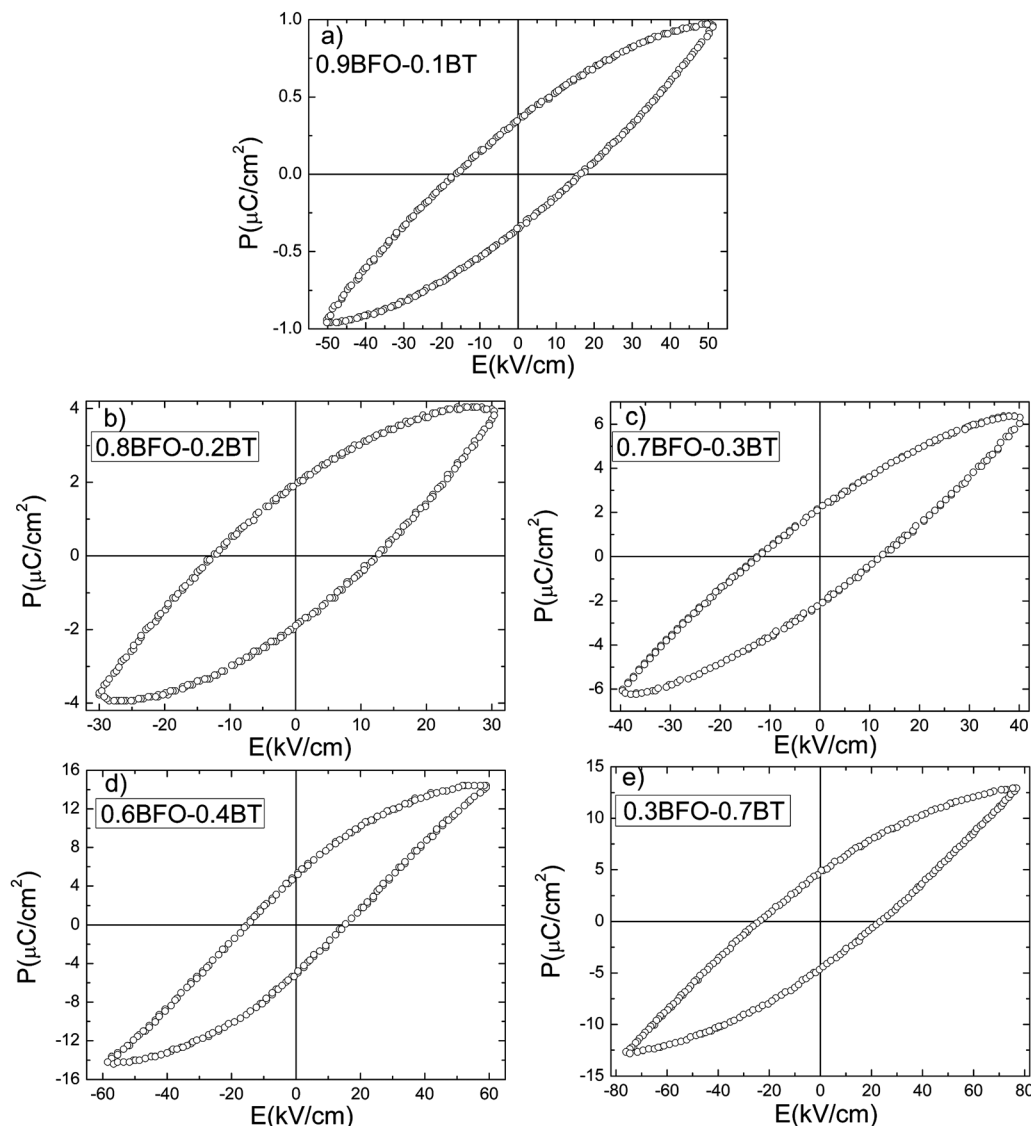

FIG. 4. Ferroelectric hysteresis loops for (x)BiFeO$_3$–(1-x)BaTiO$_3$ ceramics at room temperature and 10 Hz.

leads to the coexistence of two distinct structural symmetries. For high BF concentrations, the polarization of these two symmetries are competing and, as the BT content increases, the *Cm* symmetry became the dominant one, allowing the observation of high polarizations. Further addition of BT causes an symmetry increase, as observed in Figs. 3(a) and 3(b), and a reduction in the polarization (Fig. 3(d)).

The magnetic hysteresis loops for BF–BT solid solutions, for $0.9 \geq x \geq 0.3$, are shown in Figs. 5(a) and 5(b). All samples presented small remnant magnetizations, without saturation. The observed magnetizations are presumably due to the canted antiferromagnetic order of Fe–O–Fe spin chains.[35,36] This fact attests that the substitutions of Bi and Fe by Ba and Ti, respectively, were able to break the cycloidal spin structure of the BF matrix, releasing the macroscopic magnetization and leading to a weak ferromagnetic order. The remnant magnetization (M_R) and the coercive field (E_C) parameters are near the same for 0.9BF–0.1BT, 0.8BF–0.2BT, and 0.7BF–0.3BT compositions, and were found around 0.025 emu/g and 0.08 T, respectively. These results are in accordance with those reported in literature,[19,35,36] where the 0.8BF–0.2BT solid solution presented the highest M_R.
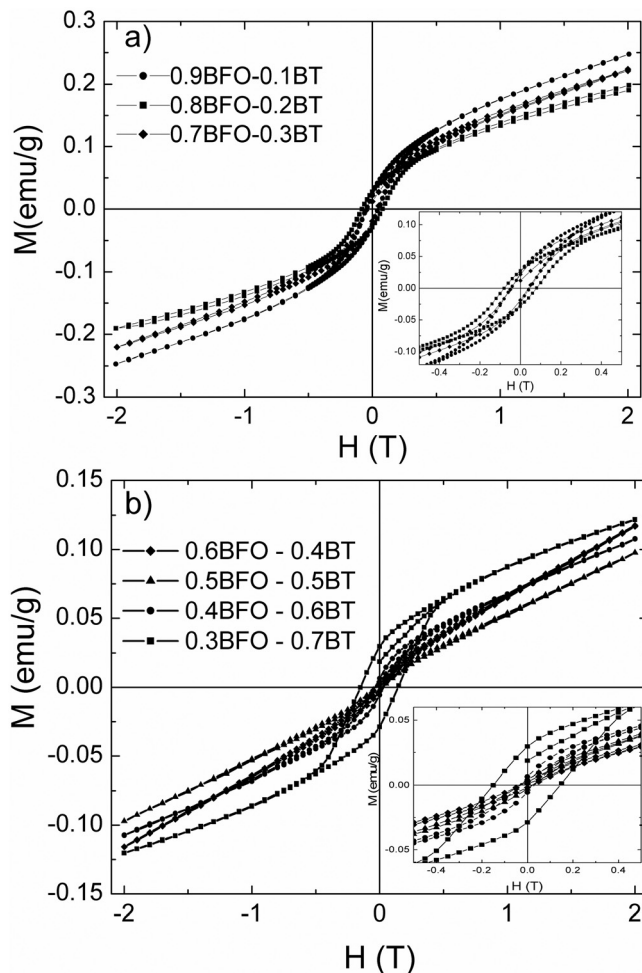
As the BT content increases, the M_R values and the area enclosed by the hysteresis loops decreases. This is due to the reduction of the Fe–O–Fe spin chains promoted by the ion substitutions. This feature can be viewed in Fig. 3(d). However, beyond the maximum M_R, observed for the 0.8BF–0.2BT sample, there is a minimum M_R value for the 0.5BF–0.5BT sample. After that, the M_R values increase continuously. It was also observed a change in the hysteresis loop shape and in the coercive field for the 0.3BF–0.7BT sample, suggesting some changes in the magnetic behavior of this sample. For checking these changes, Arrot plots (M^2 *versus* M/H curves) were constructed by using the magnetization curves of the BF–BT solid solutions (see Fig. 6). As can be observed, for high BF concentrations, the Arrot plots in high magnetic fields are parallel to each other, revealing similar magnetic behaviors in this composition range.[37,38] When the BT concentration reaches 60%, the Arrot plots are no longer parallel to that ones for high BF concentrations, revealing and attesting the different magnetic behavior between high and low BF concentrated BF–BT solid solutions.

Mössbauer spectral studies also reveal different magnetic behaviors for BF–BT samples as a function of the BT content (Figs. 7(a) and 7(b)). The Mössbauer parameters are listed in Table I. For high BF concentration samples, the Mössbauer spectra were very similar to those found for pure BF.[36] The spectra that shows a magnetic spectral signature which corresponds to ordered Fe^{3+} ions in two crystallographic environments, with dissimilar electric field gradients.[36] These features are evidenced in Fig. 7(a), where the Mössbauer spectrum for the 0.8BF–0.2BT sample was fitted with two sextets of closer magnetic hyperfine fields ($B_{HF} = 48.7$ and 48.1 T, respectively), and very different quadrupolar splitting ($\Delta_{EQ} = 0.30$ and -0.04 mm/s). Also, the obtained isomer shifts (IS = 0.45 and 0.36 mm/s) indicate only the existence of Fe^{3+} ions in both solid solutions.[39] The other compositions, with high BF concentrations, presented similar results. Specially, we obtained B_{HF} values of 47.5 and 47.9 T, for the 0.9BF–0.1BT composition, and 47.9 and 48.4 T, for the 0.7BF–0.3BT sample.

In addition to the two sextets used to fit the Mössbauer spectra of high-concentrated BF samples, a doublet was also
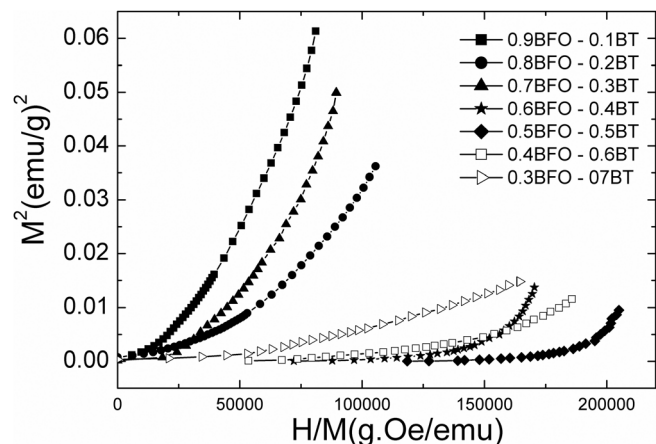
FIG. 5. (a) and (b) magnetic hysteresis loops for (x)BiFeO$_3$–(1-x)BaTiO$_3$ ceramics at room temperature.

FIG. 6. Arrot plots for the (x)BiFeO$_3$–(1-x)BaTiO$_3$ solid solutions at room temperature.
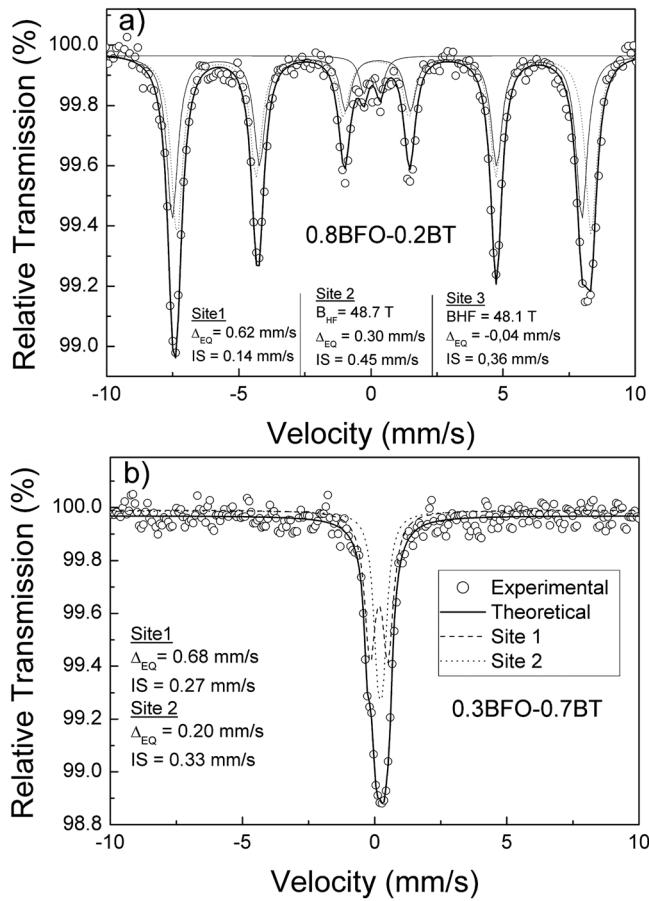
FIG. 7. Mössbauer spectra (open circles) for (a) $0.8BiFeO_3$–$0.2BaTiO_3$ and (b) $0.3BiFeO_3$–$0.7BaTiO_3$ solid solutions at room temperature. The line through the data is the fitted spectrum. The dashed and dotted lines correspond to the fitted subspectra.

observed and used for adequately fit these spectra. This doublet corresponds to a small part of the total spectrum and its Δ_{EQ} and IS parameters, indicating that this subspectrum corresponds to Fe^{3+} ions in a noncentrosymmetric environment. With increasing the BT content the doublet contribution increases, and the B_{HF} corresponding to both sextets diminish until 43.5 and 43.4 T, for the 0.5BF–0.5BT composition, and 39.3 and 40.7 T, for the 0.4BF–0.6BT sample, respectively. When the BT concentration reaches 70%, the Mössbauer spectrum exhibits only a quadrupolar signature consistent with a paramagnetic state. Fig. 7(b) shows the Mössbauer spectrum for the 0.3BF–0.7BT solid solution and the fitted results (two discrete doublets). The Δ_{EQ} and IS parameters were found as 0.68 mm/s and 0.27 mm/s, respectively, for the first ferrous site, and 0.20 mm/s and 0.33 mm/s for the second one.

By comparing Mössbauer, magnetization, and Rietveld refinement results it is seen that the overall characteristics of the Mössbauer spectra clearly reveal a transformation from an ordered spin structure of Fe^{3+} ions, for high BF concentrations, to a disordered one at low BF concentrations. This strongly indicates that the Fe ions do not contribute to the magnetic response of those solid solutions with low BF concentrations. Actually, recent reports[40,41] show that oxygen vacancies and structural constraints, as monoclinic phases, can lead to the formation of Ti^{3+} states in BT and $FeTiO_3$. This way, the same can be hypothesized for low BF concentrated BF-BT solid solutions. In fact, the Ti^{3+} formation can explain the data for M_R in Fig. 3(d) and the differences in the magnetization curves for those samples with high and low BF concentrations. In addition, the concentrations of the *Cm* (monoclinic symmetry) and ferrous paramagnetic phases increase with the increase of the BT content. Thus, the doublets observed in the Mössbauer spectra can be associated

TABLE I. Mössbauer hyperfine parameters determined from the spectral adjustment.

(x)BF–(1-x)BT	Subspectrum	B_{Hf}(T)	ΔEq (mm/s) (±0.02)	IS (mm/s) (±0.02)	Area (%) (±0.1)
	Sextet	47.5	−0.07	0.33	46
x = 0.9	Sextet	47.9	0.34	0.46	52
	Doublet		0.52	0.16	2
	Sextet	48.1	−0.04	0.36	45
x = 0.8	Sextet	48.6	0.30	0.45	51
	Doublet		0.61	0.14	4
	Sextet	47.9	−0.10	0.33	42
x = 0.7	Sextet	48.4	0.31	0.43	52
	Doublet		0.45	0.15	6
	Sextet	47.6	−0.10	0.26	26
x = 0.6	Sextet	48.0	0.24	0.46	66
	Doublet		0.55	0.25	8
	Sextet	43.5	−0.10	0.32	27
x = 0.5	Sextet	43.4	0.20	0.41	29
	Doublet		0.46	0.15	44
	Sextet	39.3	0.03	0.15	27
x = 0.4	Sextet	45.7	0.17	0.45	21
	Doublet		0.51	0.43	9
	Doublet		0.44	0.29	43
x = 0.3	Doublet		0.67	0.27	58
	Doublet		0.20	0.32	42

with the *Cm* phase since any secondary phases, which could be attributed to the observed doublets, were identified in the XRD analyzes.

IV. CONCLUSIONS

The coexistence of *R3c* and *Cm* perovskite structured phases in the BF–BT solid solutions was observed. This coexistence is due to the competition between two different mechanisms that are responsible for ferroelectricity in BF and BT compounds. By increasing the BT content in BF–BT solid solutions the *Cm* phase becomes major, and for high BT concentrations the solid solutions approach to the tetragonal symmetry, as observed in the lattice parameters behavior. The ferroelectric and magnetic properties are also strongly affected by the addition of BT into the BF matrix. For high BF concentrated samples, the observed polarizations are very small when compared to those expected for pure BF. Magnetization decreases with the increase of BT content until 50%, where magnetization starts to increase again. The 0.3BF–0.7BT sample presents a magnetization close to that of high BF concentrated samples, and a dissimilar magnetic behavior not centered in Fe ions emerges. In fact, these results clearly indicate that Ti ions are contributing for both magnetization and polarization in this sample.

ACKNOWLEDGMENTS

[1]N. A. Spaldin, Science **309**, 391 (2005).
[2]H. Schmid, Ferroelectrics **162**, 317 (1994).
[3]I. E. Dzyaloshinskii, Sov. Phys. JETP **10**, 628 (1959).
[4]C. Ederer and C. J. Fennie, J. Phys.: Condens. Matter **20**, 434219 (2008).
[5]W. Erenstein, N. D. Mathur, and J. F. Scott, Nature **442**, 759 (2006).
[6]M. Fiebig, J. Phys. D: Appl. Phys. **38**, R123 (2005).
[7]D. Lebeugle, D. Colson, A. Forget, M. Viret, A. M. Bataille, and A. Gukasov, Phys. Rev. Lett. **100**, 227602 (2008).
[8]J. R. Teague, R. Gerson, and W. James, Solid State Commun. **8**, 1073 (1970).
[9]I. Sosnowska, T. Peterlin-Neumaier, and E. Steichele, J. Phys. C: Solid State Phys. **15**, 4835 (1982).
[10]P. Fischer, M. Polomska, I. Sosnowska, and M. Szymanski, J. Phys. C **13**, 1931 (1980).
[11]N. A. Hill, J. Phys. Chem. B **104**, 6694 (2000).
[12]D. Khomskii, J. Magn. Magn. Mater. **306**, 1 (2006).
[13]S. Cheong and M. Mostovoy, Nature Mater. **6**, 13 (2007).
[14]I. M. Sosnowska, J. Microscopy **236**, 109 (2009).
[15]R. A. M. Gotardo, L. F. Cótica, I. A. Santos, E. Botero, D. Garcia, and J. A. Eiras, Scr. Mater. **61**, 508 (2009).
[16]V. F. Freitas, L. F. Cótica, I. A. Santos, D. Garcia, and J. A. Eiras, J. Eur. Ceram. Soc. **31**, 2965 (2011).
[17]L. F. Cótica, F. R. Estrada, V. F. Freitas, G. S. Dias, I. A. Santos, J. A. Eiras, and D. Garcia, J. Appl. Phys. **111**, 114105 (2012).
[18]M. M. Kumar, A. Srinivas, and S. V. Suryanarayana, J. Appl. Phys. **87**, 855 (2000).
[19]J. S. Kim, C. Cheon, C. Lee, and P. Jang, J. Appl. Phys. **96**, 468 (2004).
[20]T. Ozaki, S. Kitagawa, S. Nishihara, Y. Hosokoshi, M. Suzuki, Y. Noguchi, M. Miyayama, and S. Mori, Ferroelectrics **385**, 155 (2009).
[21]Y. Wei, X. Wang, J. Jia, and X. Wang, Ceram. Int. **38**, 3499 (2012).
[22]P. Ravindran, R. Vidya, A. Kjekshus, H. Fjellvåg, and O. Eriksson, Phys. Rev. B. **74**, 224412 (2006).
[23]O. E. Gonzalez–Vazquez and J. Íñiguez, Phys. Rev. B **79**, 064102 (2009).
[24]G. Catalan and J. F. Scoot, Adv. Mater. **21**, 1 (2009).
[25]S. Bhattacharjee, V. Pandey, R. K. Kotnala, and D. Pandey, Appl. Phys. Lett. **94**, 012906 (2009).
[26]R. Kiyanagi, T. Yamazaki, Y. Sakamoto, H. Kimura, Y. Noda, K. Ohyama, S. Torii, M. Yonemura, J. Zhang, and T. Kamiyama, Jpn. J. Appl. Phys. **81**, 024603 (2012).
[27]B. Noheda, J. A. Gonzalo, L. E. Cross, R. Guo, S.-E. Park, D. E. Cox, and G. Shirane, Phys. Rev. B **61**, 8687 (2000).
[28]B. Noheda, D. E. Cox, G. Shirane, S.-E. Park, L. E. Cross, and Z. Zhong, Phys. Rev. Lett. **86**, 3891 (2001).
[29]D. S. F. Viana, R. A. M. Gotardo, L. F. Cótica, I. A. Santos, D. Garcia, J. A. Eiras, M. Olzon-Dyonysio, S. D. Souza, and A. A. Coelho, J. Appl. Phys. **110**, 034108 (2011).
[30]J. Rodriguez-Carvajal, Physica B **192**, 55 (1993).
[31]L. F. Cótica, V. F. Freitas, G. S. Dias, R. A. M. Gotardo, I. A. Santos, D. Garcia, and J. A. Eiras, Integr. Ferroelectr. **131**, 230 (2011).
[32]M. M. Kumar, V. R. Palkar, K. Srinivas, and S. Suryanarayana, Appl. Phys. Lett. **76**, 2764 (2000).
[33]A. K. Pradhan, K. Zhang, D. Hunter, J. B. Dadson, G. B. Loutts, P. Bhattacharya, P. Katiyar, J. Zhang, D. J. Sellmyer, U. N. Roy, Y. Cui, and A. Burger, J. Appl. Phys **97**, 093903 (2005).
[34]H. Yang, Q. Ke, H. Si, and J. Chen, J. Appl. Phys **111**, 024104 (2012).
[35]M. M. Kumar, S. Srinath, G. S. Kumar, and S. V. Suryanarayana, J. Magn. Magn. Mater. **188**, 203 (1998).
[36]T. Park, G. Papaefthymiou, A. Viescas, Y. Lee, H. Zhou, and S. Wong, Phys. Rev. B **82**, 024431 (2010).
[37]A. Arrot, Phys. Rev. **108**, 1394 (1957).
[38]I. Yeung, R. M. Roshko, and G. Williams, Phys. Rev. B **34**, 3456 (1986).
[39]G. J. Long and F. Grandjean, *Mössbauer Spectroscopy Applied to Magnetism and Materials Science* (Plenum, New York, 1996), Vol. 2.
[40]R. V. K. Mangalam, N. Ray, U. Waghmare, A. Sundaresan, and C. N. Rao, Solid State Commun. **149**, 1 (2009).
[41]S. Banerjee, A. Datta, A. Bhaumik, and D. Chakravorty, J. Appl. Phys. **110**, 064316 (2011).